

# Semi-Automated Workflow for Computer-Generated Scoring of Ki67 Positive Cells from HE Stained Slides

Dominika Petříková<sup>1,2</sup><sup>a</sup>, Ivan Cimrák<sup>1,2</sup><sup>b</sup>, Katarína Tobiášová<sup>3</sup> and Lukáš Plank<sup>3</sup><sup>c</sup>

<sup>1</sup>*Cell-in-fluid Biomedical Modelling & Computations Group, Faculty of Management Science and Informatics, University of Žilina, Slovak Republic*

<sup>2</sup>*Research Centre, University of Žilina, Slovak Republic*

<sup>3</sup>*Department of Pathology, Jessenius Medical Faculty of Comenius University and University Hospital, Martin, Slovak Republic*

**Keywords:** Hematoxylin and Eosin, Ki67, Clustering, Neural Networks, Digital Pathology.

**Abstract:** The Ki67 positive cell score assessed by immunohistochemistry (IHC) is considered a good biomarker of cell proliferation in determining therapeutic protocols. Manual estimation of Ki67 scores has several limitations as it is time consuming and subject to inter-rater variability. Moreover, the IHC staining is not always available. This could potentially be addressed by using neural network models to predict Ki67 scores directly from hematoxylin and eosin (HE) stained tissue. However, neural networks require large well-annotated datasets, the creation of which is often a laborious process requiring the work of experienced pathologists. Such database containing images of HE stained tissue with Ki67 labels is currently not available. In this paper, we propose a semi-automated dataset generation approach to predict Ki67 scores from pairs of HE and IHC slides with minimal assistance from experts. Using a sample of 15 pairs of whole slide images stained by HE and IHC methods, we proposed a workflow for generating HE patches with Ki67 labels using image analysis methods such as clustering and tissue registration. From the IHC images processed by the aforementioned methods, we estimated the percentage of Ki67 positive cells in each patch. To verify the validity of the proposed approach we automatically assigned Ki67 labels to HE patches from manually annotated HE - Ki67 pairs. To illustrate the potential of neural network for assigning the Ki67 label to HE patches, we trained a neural network model on a sample of three whole slide images, which was able to classify Ki67 positivity ratio of tissue from HE patches into two Ki67 labels.

## 1 INTRODUCTION

In clinical settings, histopathology images are a critical source of primary data for pathologists to perform cancer diagnostic. Digital slide scanners allow to digitize histology slides into high-resolutions images. This generates vast amounts of data which if automatically processed gives the opportunity to employ machine learning algorithms for e.g. classification of the specimen (He et al., 2012; Pantanowitz, 2010).

Histopathology analysis is performed using sections of tissue, with most common hematoxylin and eosin (HE) staining. Additional immunochemistry (IHC) labeling may be performed to obtain addi-

tional information (Xu et al., 2019). Example of stained tissue sections are displayed in Figure 1. The histopathological diagnosis of a malignant neoplasia includes evaluation of its grading (grade of malignancy) based on the evaluation of various tumor parameters. One of the most important parameters is the tumor proliferation rate represented by the percentage of tumor cells showing intranuclear positivity by IHC using Ki67 monoclonal antibody (Li et al., 2015; Kos and Dabbs, 2016). This is especially true for neuroendocrine neoplasias (NENs). The traditionally world-wide accepted grading of NENs recognizes three grades: G1 with less than 3%, G2 with 3-20% and G3 more than 20% of Ki67 positive tumor cells. The G3 NENs which include all tumors with Ki67 positivity within the interval of 20-100% of the cells show clinically a bright spectrum of aggressive behaviour. Based on this evidence the attempts

<sup>a</sup> <https://orcid.org/0000-0001-8309-1849>

<sup>b</sup> <https://orcid.org/0000-0002-0389-7891>

<sup>c</sup> <https://orcid.org/0000-0002-1153-1160>

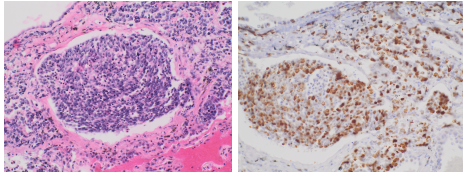


Figure 1: Example of tissue section stained with HE and IHC Ki67.

are on the horizon to stratify G3 NENs into two new (sub-)categories using a threshold of 40-50% tumor cells positivity. The ambition to make this stratification precise and accurate is in contrast with the intra- and interobserver variability by routine histopathologic evaluation of Ki67 proliferation activity. Therefore the scoring of Ki67 positive cells from basic HE staining would bring a significant advantage during the evaluation of HE stained images (Boukhar et al., 2021; Satturwar et al., 2020).

The IHC labelling is frequently performed on different slides adjacent to HE stained slides. This allows pathologists to easily compare regions of a HE and adjacent IHC slides. Even though the adjacent samples are still showing similar spatial characteristics, they are not identical to the other samples and they can be shifted and rotated. To perform machine learning data analysis and interpretation, it is critical to align these differently stained histopathology images together.

Machine learning algorithms proved to uncover hidden features in images that contribute to classification of the images (Klimo et al., 2016; Klimo et al., 2021; Ondrašovič and Tarábek, 2021). Training a machine learning model for image segmentation requires a large amount of high-quality, annotated images as a training dataset. The difficulty of these annotations in terms of both the rater's expertise and the effort required to create increases sharply between whole slide-level, region-level, and cell-level analyses.

Whole-slide annotations may be easier to obtain, but the use of such weak-annotated datasets is quite limited. The goal is usually to identify patches that can collectively or independently predict the whole slide label. For example, (Zhu et al., 2017; Yue et al., 2019) used k-means clustering and found the most discriminative clusters of patches by training CNNs in a weakly supervised manner.

Cell-level annotations are either extremely demanding for the raters or require an intermediate step of cell segmentation and afterwards the use of region-level annotations. Cell segmentation has been successfully used e.g. to segment white blood cell, their nuclei and the surrounding cytoplasm (Al-Dulaimi et al., 2021). Valuable dataset of segmented blood cells has been recently published (Kouzehkanan et al.,

2022). Segmentation methods however require careful tuning of model parameters that makes them less robust than region-level annotations.

Region-level annotations require more input from the experts however it is still reasonable and we will further explore this approach. Using region annotations, one can typically generate rectangular patches each with its own label that can serve directly as inputs into machine learning algorithms. This approach has been used in (Abousamra et al., 2021) where authors fine-tuned VGGNet, ResNet and InceptionV4 models to get probabilities of small patches (100x100 pixels) being tumor infiltrating lymphocytes positive or negative. The patches were extracted from whole slide images of 23 cancer types. Authors in (Hameed et al., 2020) compared accuracy of stand-alone VGG-16 and VGG-19 models with ensemble models consisting of both architectures in classification breast cancer histopathological images as carcinoma and non-carcinoma.

Many recent studies showed that there exists correlation between HE and IHC staining, specifically for hormonal receptors such as estrogen, progesteron or Her2 receptors (Naik et al., 2020; Rawat et al., 2020). In (Liu et al., 2020), authors addressed the problem of double staining in determining the number of Ki67 positive cells for cancer treatment. Employing matching pairs of IHC and HE-stained images, three different neural networks were used to produce a heat map of higher Ki67 concentration on the whole slide image. Here, cell segmentation step has been used during the workflow to obtain annotated cell patches from homogeneous Ki67 positive or negative regions. Another approach of obtaining annotated cell images was presented in (Sheikhzadeh et al., 2016), where authors trained a CNN model to classify biomarkers from IHC images. Such a model could potentially be used to automatically annotate large amounts of data, but training NN model required segmentation of cells and subsequent manual annotation by experts.

## Contents of This Work

In this work we aim at exploring the possibility to predict Ki67 protein expression from HE images. We first describe the workflow of dataset creation and then we show proof-of-concept results of neural network classification.

The dataset will consist of patches each with its individual label representing the amount of Ki67 protein expressed on that patch. To obtain the patch label, we first create aligned pair of two whole slide images, one with HE staining and one with Ki67 staining. As-

suming the spatial proximity of the physical slides from which HE and Ki67 images were obtained, we work with the assumption that a patch from the HE whole slide image can be labelled by the patch from the Ki67 whole slide image from the same location. To obtain the label from the Ki67 patch we use advanced image processing methods to determine how much of the patch area represent the Ki67 positive cells relative to area representing all cells on Ki67 patch.

In Section 2 we describe laboratory and image analysis methods. First we describe laboratory protocols for sample and image acquisition and consecutive data preprocessing. Then we present steps leading to aligning the HE and Ki67 images. The end of the section is devoted to color clustering of Ki67 images to distinguish between Ki67 positive and negative images leading to the labelling of HE patches with Ki67 labels.

In Section 3 we first validated the Ki67 labelling method on manually annotated images. Then we present results of the keypoints algorithm on aligning the HE and Ki67 images. Further we give details of color clustering and consecutive Ki67 quantification on the 15 WSI samples. Finally, we present proof-of-concept results of a simple classification of HE patches into two Ki67 labels.

## 2 METHODS

### 2.1 Image Acquisition

Formalin-fixed and paraffin-embedded specimens of pulmonary G3 NENs of 15 patients were collected from archives of Department of Pathological Anatomy JFMED CU and UH Martin. 3-4mm thick paired parallel sections of each of the cases were prepared and stained – the first by routine hematoxylin-eosin (HE) and the second by IHC with Ki67 monoclonal antibody.

Immunohistochemical analysis was performed with the EnVision FLEX High pH (Link) K8000 kit after deparaffinization of sections, using monoclonal mouse antibody clone MIB-1 (FLEX, Dako), on automatized platform PTLINK (Dako, Denmark A/S), revitalized in solution HpH (pH=9) in temperature 97°C for 20 minutes, followed by IHC reaction in AutoStainer Link 48 (Dako, Denmark). Visualization was performed using EnVision FLEX/HRP (Dako), DAB (EnVision FLEX, Dako) and contrast hematoxylin staining. The slides were first routinely evaluated by two experienced and trained pathologists to determine the percentage of Ki67 positive tumor cells.

Then the identical HE and Ki67 slides were paired together and scanned using 3D Histech PANORAMATIC© 250 Flash III 3.0.3, in BrightField Default mode.

Data have been saved in standard DICOM format.

### 2.2 Data Preprocessing

All whole slide image (WSI) files were transformed into PNG images in Python with OpenSlide library. In general, the tissues on the slides are rotated differently and HE scans contain several tissue sections. Therefore, from the slides, only-tissue cutouts were created and transformed to PNG without loss of resolution. The resulting images were approximately 20,000x20,000 pixels in size.

### 2.3 Registration with Keypoints

The tissues on the slides were rotated differently when scanned with the microscope and placed at different positions on the slide, so the tissue cutouts were not matching. First, it was necessary to find the transformation between pairs of images, that is, to find the relative degree of rotation and shifting. To do this, we used algorithm to detect keypoints. Matching features across different images is a common problem in computer vision. When two images are similar meaning they have same scale and orientation, simple corner detectors can work. However, when there is need to match images of different scales and rotations, it is necessary to use different approach. SIFT (Scale-invariant feature transform) is a keypoint detection and description algorithm invariant to rotation, shifting, scaling, illumination change and partial distortion of the object. In general, the SIFT algorithm can be decomposed into four main steps:

- Scale-space peak detection
- Keypoint localization
- Orientation assignment
- Keypoint descriptor and matching

The scale space of an image is a function produced from the convolution of a blurring referred to as gaussian kernel (or gaussian blur operator) at different scales with the input image. Scale-space is separated into octaves, so each octave's image size is half the previous one. Images, within an octave, are progressively blurred using the Gaussian blur operator applied to each pixel and

blurred images are then used to generate the difference of Gaussian obtained as the difference of images in the same octave. The resulting scale space

is searched for locale extremes. A point is selected as a local extreme if it is greater or lesser than all neighbouring points. The found local extrema are considered as potential keypoints, which are best represented in the scale in which they were a local extreme. Subsequently those keypoints that have low contrast or lie on the edge are removed. The others are considered to be strong keypoints and are retained for the calculation of descriptors.

To make the keypoints invariant to rotation, the orientation of the keypoint is computed based on its local properties. This can produce multiple keypoints that are at the same position, with the same scale, but different orientations. The next step creates descriptors and ensures their invariance to 3D rotation and illumination change. Keypoints are then matched with keypoints of another image by identifying their nearest neighbors. The nearest neighbor is the keypoint that has the shortest distance descriptor (Lowe, 2004).

## 2.4 K-Means Clustering

In order to evaluate the ratio of brown and blue pixels and so estimate the ratio of Ki67 positive cells, the whole image needs to be recoloured in the following three main colours:

- white - background
- blue - Ki67 negative
- brown - Ki67 positive.

We used a clustering algorithm to assign each pixel to one of the main colors. Clustering is an unsupervised learning technique used in many fields, including data mining, machine learning, pattern recognition and image analysis. It is a process of partitioning a data set into subsets based on similarity according to some defined distance metric or finding a structure in a collection of unlabeled data. Therefore objects in one cluster are "similar" with each other and "dissimilar" to the objects belonging into other clusters (Madhulatha, 2012).

Among the various existing clustering algorithms, we used generally the most known, K-means clustering. K-means algorithm is one of the partitioning methods. It distributes  $n$  objects in a data set  $D$  into  $k$  clusters,  $C_1, \dots, C_k$ , that is,  $C_i \subset D$  and  $C_i \cap C_j = \emptyset$ . To assess the partitioning quality, objective function that aims for high intracluster similarity and low inter-cluster similarity is used. So objects within a cluster are similar to one another but dissimilar to objects in other clusters. Centroid of a cluster is its center point and is used to represent that cluster in centroid-based partitioning techniques. It can be computed in various ways, for example by the mean or medoid of all points

assigned to the cluster. The quality of a cluster can be measured by the within-cluster variation, which is the sum of squared error (distance) between all objects in  $C_i$  and the centroid  $c_i$ , defined as:

$$E = \sum_{i=1}^k \sum_{p \in C_i} dist(p, c_i)^2, \quad (1)$$

where  $E$  is the sum of the squared error and  $dist(p, c_i)^2$  is difference between object  $p$  and centroid  $c_i$  measured as Euclidean distance of two points.

In K-means algorithm, the centroid of a cluster is defined as a mean value of the points within the cluster. First, it randomly selects  $k$  objects as initial cluster centroids or centers. All remaining objects are then assigned to the cluster, which is the most similar based on the Euclidean distance between the object and the centroid of clusters. For each cluster, new mean is computed using the objects assigned to the cluster. The algorithm then iteratively reassigns objects to the clusters with new means until the assignment is stable. K-means algorithm can be summarized as follows:

1. arbitrarily choose  $k$  objects from  $D$  as the initial cluster centers;
2. **repeat**
3. (re)assign each object to the cluster to which the object is the most similar
4. update the cluster centroids
5. **until** no change;

K-means algorithm requires the number of clusters to be determined in advance, which is perceived as a drawback in many cases (Han et al., 2012).

## 3 RESULTS

### 3.1 Validation

To validate suggested approach, we were provided with several pairs of images of identical tissues both stained with Ki67 protein. In this case, all cells in one image were crossed out with a blue or red line, depending on whether the cell was Ki67 positive or negative. This was done manually by expert pathologists and so we have known exact ratio of positive and negative cells, which we could compare to ratio obtained by our approach. Since these images are at a much lower resolution compared to the original WSIs, it was possible to perform experiments on them to adjust the parameters of the clustering algorithm such as the number of clusters and the color space in which it

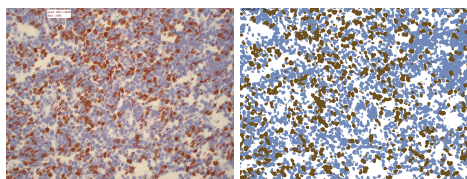


Figure 2: Example of ratio estimation on validation data.

will be applied. To determine the number of clusters, we used the elbow method, where for different values of  $k$ , the sum of the distances of all points from the centroids of the clusters in which they are included is observed. A suitable value is considered to be one where is the elbow of the curve and the sum of distances begins to converge smoothly to some value. We have applied the same approach in the RGB (Red Green Blue), HSV (Hue Saturation Value) and Lab color spaces. The only space in which an elbow could be observed was the HSV space, and this was at a value of 6 clusters, so we continued to use this value.

In Figure 2 there is example of original image with crossed cells and corresponding result of clustering with quantified ratio. In total, we compared the ratio of the 44 available images, with resulting mean error of 5.22%, which was considered acceptable.

### 3.2 HE - Ki67 Registration

Before patch generation could begin, the first necessary step was to ensure that pairs of patches from the same region of the images showed the same tissue stained differently, thus creating pairs of approximately "identical" HE and IHC images, since the tissues on the slides were rotated differently and were located at different locations on the slide. Therefore, we first made tissue cutouts from the slides as part of the image preprocessing. At the moment, the registration is done manually under the supervision of experienced medical practitioners. The procedure consisted of placing the two images, which we made slightly transparent, at the same coordinates in a suitable graphics tool and then rotating and shifting one of them until an approximate visual match of the two tissues was obtained, knowing the values of the degree of rotation and shifting. The examples of the manual registration can be seen in Figure 3.

To make this approach more automatic, we also tried to register these through key points using the SIFT algorithm. We transformed the images to grayscale and reduced the resolution from the original size by almost 50 times, but the registration was not successful. The individual tissue sections are too dissimilar despite the general similarity in shape. We tried to reduce this dissimilarity by transforming the image into a black-and-white mask through thresh-

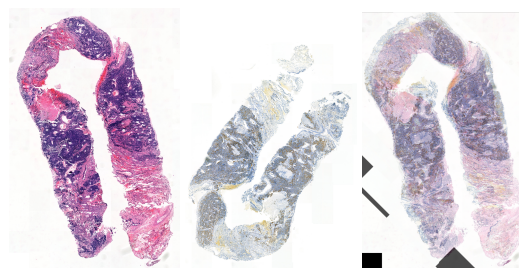


Figure 3: Manual registration.

olding methods and then applied several iterations of erosion and dilation to them with different kernel sizes. However, this did not have the desired effect only for one pair we were able to find matching key-points. Registration was successful for three pairs of scans only after applying blurring to both images. In Figure 4, the result of the registration before and after applying the blur can be seen, with the red lines connecting the paired keypoints.

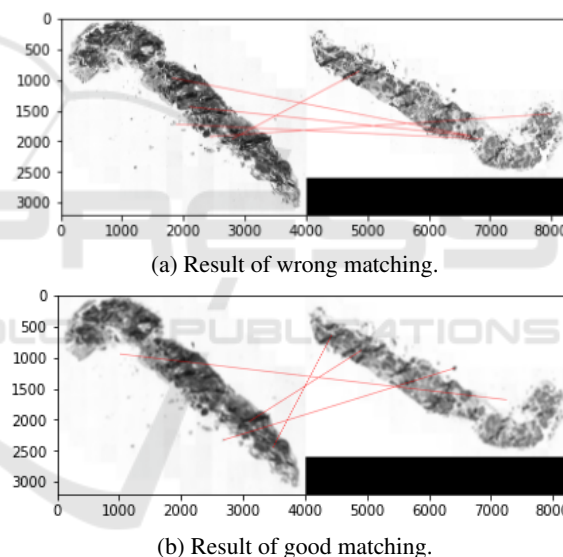


Figure 4: Example of wrong and good matching of key-points.

From the application of automatic registration on 8 images, it is likely that automatic registration can be performed for tissues that have a very specific, distinct and easily identifiable shape assuming the correct image preprocessing parameters are found, otherwise this approach is not very successful yet and needs to be further investigated. In addition, trying different image and parameter adjustments is often more time consuming than manual registration. Simplifying the automatic registration could be helped by ensuring that the tissue sections stained by HE and Ki67 are sections created right after each other and thus the tissue on them would match more closely.

### 3.3 Color Clustering

As a first approach, we thought that recolouring the IHC images would also be possible based on colour analysis through histograms, which would allow us to find the dominant colours of the image. The output would be threshold values according to which all pixels would be recoloured. However, after displaying the histograms for each color channel, we were unable to determine any dominant colors other than white and therefore rejected this method. Instead, we used a clustering method, namely K-means, to create clusters of pixels with similar color. We set the parameter  $k$  according to the results of the experiments on the validation data and applied the method in the HSV color space. Due to insufficient memory capacity, it was not possible to perform clustering on the whole WSIs, so we divided each image into 4 parts and applied the clustering method to them separately.

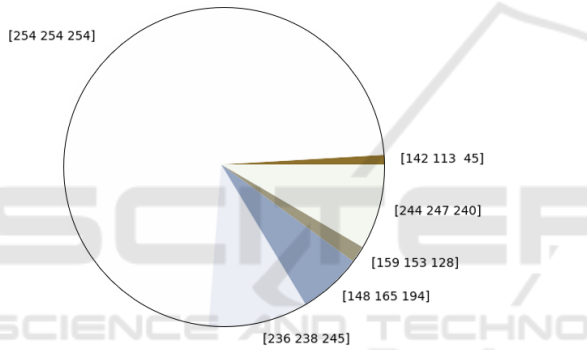


Figure 5: Pie chart of centroid from clustering colors.

The resulting cluster's centroids were transformed into RGB space and displayed them in a pie chart, which is shown in Figure 5. It was then necessary to perform a visual analysis and expertly determine under the supervision of medical practitioners, which centroid would belong to which category (background, Ki67 positive, Ki67 negative). Finally, all pixels were recolored according to their association with given cluster and centroid into one of the three specified colors as is displayed in Figure 6.

### 3.4 Ki67 Quantification

To determine the score of Ki67 positive cells, we quantified the ratio of the number of pixels stained with the color corresponding to a Ki67 positive cell (brown), to all pixels that have any cell (are brown or blue) as follows:

$$ratio = \frac{brownpixels}{brownpixels + bluepixels} \quad (2)$$

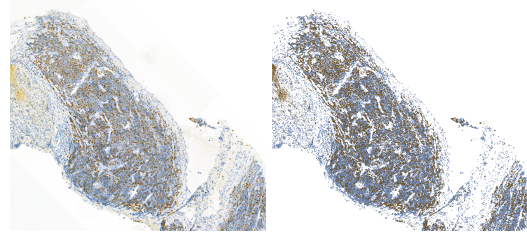


Figure 6: Comparison of original image and recolored one after clustering.

In addition to this metric, it would also be possible to determine the ratio of positive cells (pixels of a particular color) to all pixels to account for how much of the tissue overall is occupied by Ki67-positive cells, but we have not yet addressed this. Before the quantification, the size of the patches had to be determined. On one hand, we wanted to match the size of the patches to the size of the input images of the pre-trained neural network architectures so that they did not need to be resized. On the other hand, it was necessary to take into account that the scanned tissue sections on the HE and IHC slides were not cut right after each other, resulting in them not matching at the cellular level. Therefore, the patches were not allowed to be too small, but to be of sufficient size to capture multiple cells, as we assume that the tissue structure in one area remains preserved. To verify this assumption, we generated patches of  $224 \times 224$  pixels, quantified the Ki67-positivity ratio, and plotted all patches from the image in a heatmap stained according to the degree of Ki67-positivity presented in Figure 7 and Figure 8. The aim was to verify that although the tissues are not identical, there are regions of equal intensity of Ki67 positivity from which patches can be generated, which was confirmed.

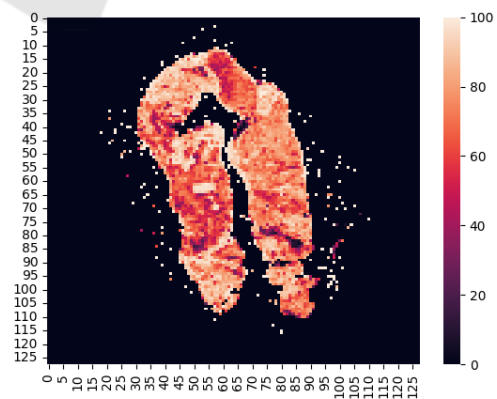


Figure 7: Heatmap of ratios intensity in  $224 \times 224$  patches.

When generating patches for classification purposes, we were only interested in patches that had at least 60% of the total area covered by cells, so we

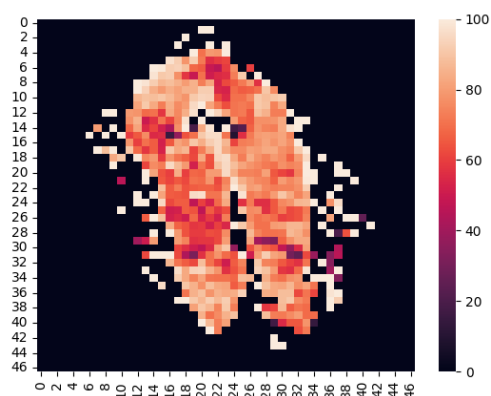


Figure 8: Heatmap of ratios intensity in 600x600 patches.

discarded all other patches. From the three WSIs, we were able to produce 2618 patches of size 224 x 224 pixels and 308 patches of size 600 x 600 pixels. For both sizes, we can see in the figure 9 the histogram of cell positivity with respect to the total cell area.

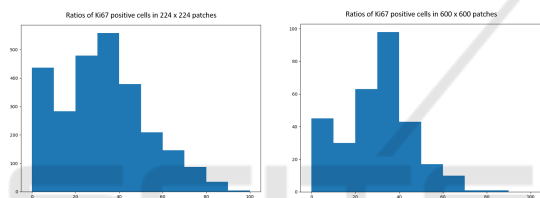


Figure 9: Histograms of Ki67 positive cells ratios in 224x224 and 600x600 pixels patches.

### 3.5 Neural Network Training

As an initial proof-of-concept to demonstrate the correctness and functionality of the proposed dataset generation approach for classification purposes, we generated patches from three WSIs and trained a neural network model to classify the ratio of Ki67 positive cells from HE stained tissue in Python with Tensorflow library. We divided the dataset into two categories according to the proportion of Ki67 positive cells. The first contained patches containing less than 30 percent and the second more than 60 percent. We omitted the values in the middle in this first experiment to make classification easier. The dataset in this case was divided into training, validation and test sets in a ratio of 8:1:1. On training set we also applied augmentation: horizontal flip, vertical flip and rotation. The frequencies of each class are shown in Table 1.

We fine-tuned the ResNet18 architecture pre-trained on the ImageNet dataset with first three residual blocks frozen, so only the last residual block and fully-connected layers were trained for 500 epochs with batch size 64. Progress of accuracy during training on train and validation set is displayed in Fig-

Table 1: Splitting of dataset.

	30-	60+
Train	1000	370
Valid	125	46
Test	126	47

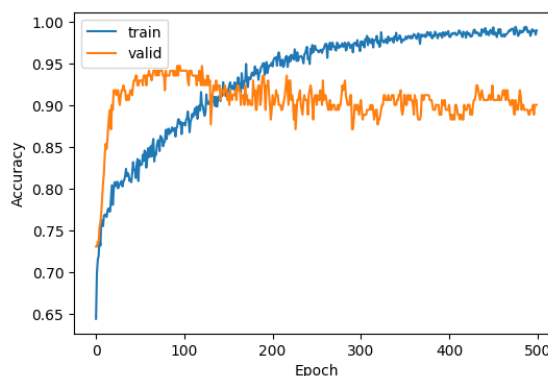


Figure 10: Progress of accuracy during training neural network.

ure 10. We retained the weights of the model that achieved the highest accuracy on the validation set, its resulting accuracy was: train 0.92, valid 0.94 and test 0.82.

## 4 CONCLUSIONS

In this paper, we made an attempt to create semi-automated workflow for estimation of Ki67 positive score from IHC stained tissue in order to predict ratio of Ki67 positive cells from HE patches. We introduced a data annotation approach that uses image analysis methods to facilitate the extraction of annotated data for the purpose of training neural networks that require large amounts of data. In contrast to (Liu et al., 2020), our dataset construction approach does not rely on the existence of homogeneous regions of Ki67 positive or negative cells from which patches of labelled cells were segmented. Moreover, proposed approach works at the WSIs level and can therefore be applied to an arbitrarily large tissue sections without need to perform cell segmentation. Nevertheless, this study has some limitations including small sample size and the need to visually detect the resulting centroids as Ki67 positive, negative or background. Additionally, due to memory and computational constraints, the clustering hyperparameters had to be determined from experiments performed on validation data, not WSIs designed for scoring. Even so, our results show that there is a possibility for automatic estimation of molecular information in IHC images,

and there is a relationship between the information thus obtained and the morphological information displayed in HE images. Moreover, initial experiments show that this relationship can be modeled by machine learning models such as neural networks.

However, it's just the beginning of our research on this topic. Challenges still exist, including:

1. The registration of tissue pairs needs to be done manually, or human intervention is needed to find the correct parameters of the automated approach, which additionally needs to be visually inspected. In the future, it would be necessary to develop an automatic registration approach also with subsequent validation of the correctness of the key-points matching.
2. The relationship between HE and IHC-stained tissue can be very complex due to the diversity of tissues, cells and antibodies used to produce IHC. Our research has so far focused on only one specific protein, Ki67, so it would be necessary to verify whether this approach works on other types of HE and IHC pairs.

Our future work will mainly focus on the following aspects. Firstly, enlarge our dataset to contain more samples, so the model trained on the new dataset will have stronger ability of generalization. In this step, we will also include new tissue samples whose HE and IHC sections followed each other immediately to ensure as much tissue identity on them as possible. Secondly, conduct more experiments and optimize our model.

## ACKNOWLEDGEMENTS

This publication has been produced with the support of the Integrated Infrastructure Operational Program for the projects "New possibilities for the management of serious diseases in medical and preventive care with regard to the safety of health professionals", ITMS:313011AUA5 and "Integrated strategy in the development of personalized medicine of selected malignant tumor diseases and its impact on life quality", ITMS code: 313011V446, both co-financed by the European Regional Development Fund.

## REFERENCES

- Abousamra, S., Gupta, R., Hou, L., Batiste, R., Zhao, T., Shankar, A., Rao, A., Chen, C., Samaras, D., Kurc, T., and Saltz, J. (2021). Deep learning-based mapping of tumor infiltrating lymphocytes in whole slide images of 23 types of cancer. *Front. Oncol.*, 11:806603.
- Al-Dulaimi, K., Banks, J., Nugyen, K., Al-Sabaawi, A., Tomeo-Reyes, I., and Chandran, V. (2021). Segmentation of white blood cell, nucleus and cytoplasm in digital haematology microscope images: A review-challenges, current and future potential techniques. *IEEE Rev. Biomed. Eng.*, 14:290–306.
- Boukhar, S. A., Gosse, M. D., Bellizzi, A. M., and Rajan K D, A. (2021). Ki-67 Proliferation Index Assessment in Gastroenteropancreatic Neuroendocrine Tumors by Digital Image Analysis With Stringent Case and Hotspot Level Concordance Requirements. *American Journal of Clinical Pathology*, 156(4):607–619.
- Hameed, Z., Zahia, S., Garcia-Zapirain, B., Javier Aguirre, J., and María Vanegas, A. (2020). Breast cancer histopathology image classification using an ensemble of deep learning models. *Sensors (Basel)*, 20(16):4373.
- Han, J., Kamber, M., and Pei, J. (2012). 10 - cluster analysis: Basic concepts and methods. In Han, J., Kamber, M., and Pei, J., editors, *Data Mining (Third Edition)*, The Morgan Kaufmann Series in Data Management Systems, pages 443–495. Morgan Kaufmann, Boston, third edition edition.
- He, L., Long, L. R., Antani, S., and Thoma, G. R. (2012). Histology image analysis for carcinoma detection and grading. *Computer Methods and Programs in Biomedicine*, 107(3):538–556.
- Klimo, M., Lukáč, P., and Tarábek, P. (2021). Deep neural networks classification via binary error-detecting output codes. *Appl. Sci. (Basel)*, 11(8):3563.
- Klimo, M., Tarábek, P., Šuch, O., Smieško, J., and Škvarek, O. (2016). Implementation of a deep relu neuron network with a memristive circuit. *International Journal of Unconventional Computing*, 12(4):319 – 337.
- Kos, Z. and Dabbs, D. J. (2016). Biomarker assessment and molecular testing for prognostication in breast cancer. *Histopathology*, 68(1):70–85.
- Kouzehkanan, Z. M., Saghari, S., Tavakoli, S., Rostami, P., Abaszadeh, M., Mirzadeh, F., Satlsar, E. S., Gheidishahran, M., Gorgi, F., Mohammadi, S., and Hosseini, R. (2022). A large dataset of white blood cells containing cell locations and types, along with segmented nuclei and cytoplasm. *Sci. Rep.*, 12(1):1123.
- Li, L. T., Jiang, G., Chen, Q., and Zheng, J. N. (2015). Ki67 is a promising molecular target in the diagnosis of cancer (review). *Mol. Med. Rep.*, 11(3):1566–1572.
- Liu, Y., Li, X., Zheng, A., Zhu, X., Liu, S., Hu, M., Luo, Q., Liao, H., Liu, M., He, Y., and Chen, Y. (2020). Predict ki-67 positive cells in H&E-stained images using deep learning independently from IHC-stained images. *Front. Mol. Biosci.*, 7:183.
- Lowe, D. G. (2004). Distinctive image features from scale-invariant keypoints. *International Journal of Computer Vision*, 60(2):91–110.
- Madhulatha, T. S. (2012). An overview on clustering methods. *CoRR*, abs/1205.1117.
- Naik, N., Madani, A., Esteva, A., Keskar, N. S., Press, M. F., Ruderman, D., Agus, D. B., and Socher, R. (2020). Deep learning-enabled breast cancer hor-

- monal receptor status determination from base-level H&E stains. *Nat. Commun.*, 11(1):5727.
- Ondrašovič, M. and Tarábek, P. (2021). Homography ranking based on multiple groups of point correspondences. *Sensors (Basel)*, 21(17).
- Pantanowitz, L. (2010). Digital images and the future of digital pathology: From the 1st digital pathology summit, new frontiers in digital pathology, university of nebraska medical center, omaha, nebraska 14-15 may 2010. *Journal of Pathology Informatics*, 1(1):15.
- Rawat, R. R., Ortega, I., Roy, P., Sha, F., Shibata, D., Ruderman, D., and Agus, D. B. (2020). Deep learned tissue “fingerprints” classify breast cancers by ER/PR/Her2 status from H&E images. *Sci. Rep.*, 10(1):7275.
- Satturwar, S. P., Pantanowitz, J. L., Manko, C. D., Seigh, L., Monaco, S. E., and Pantanowitz, L. (2020). Ki-67 proliferation index in neuroendocrine tumors: Can augmented reality microscopy with image analysis improve scoring? *Cancer Cytopathology*, 128(8):535–544.
- Sheikhzadeh, F., Guillaud, M., and Ward, R. K. (2016). Automatic labeling of molecular biomarkers of whole slide immunohistochemistry images using fully convolutional networks.
- Xu, Z., Huang, X., Moro, C. F., Bozóky, B., and Zhang, Q. (2019). Gan-based virtual re-staining: A promising solution for whole slide image analysis.
- Yue, X., Dimitriou, N., and Arandjelovic, O. (2019). Colorectal cancer outcome prediction from H&E whole slide images using machine learning and automatically inferred phenotype profiles.
- Zhu, X., Yao, J., Zhu, F., and Huang, J. (2017). WSISA: Making survival prediction from whole slide histopathological images. In *2017 IEEE Conference on Computer Vision and Pattern Recognition (CVPR)*. IEEE.